Original Article

A translational mouse model for investigation of the mechanism of preterm diffuse white matter injury

Qiufan Chen[1,2#], Ke Zhang[1,2#], Minjie Wang[1,2], Ruiwei Gao[1,2], Qian Wang[1,2], Mili Xiao[1,2], Chao Chen[1,2]

[1]Department of Neonatology, Children's Hospital of Fudan University, Shanghai, China; [2]Key Laboratory of Neonatal Disease, Ministry of Health, Shanghai, China

Contributions: (I) Conception and design: C Chen, Q Chen, K Zhang; (II) Administrative support: C Chen, M Wang, R Gao; (III) Provision of study materials or patients: Q Chen, M Wang, R Gao; (IV) Collection and assembly of data: Q Chen, Q Wang, M Xiao; (V) Data analysis and interpretation: K Zhang, M Xiao; (VI) Manuscript writing: All authors; (VII) Final approval of manuscript: All authors.

[#]These authors contributed equally to this work.

Correspondence to: Chao Chen, PhD. Department of Neonatology, Children's Hospital of Fudan University, Shanghai 201102, China. Email: chaochen@fudan.edu.cn.

Background: The increasing incidence of preterm birth has led to a global problem of adverse neurodevelopmental outcomes in preterm neonates as a result of brain injury. There is still a lack of models mimicking diffuse white matter injury (WMI) in preterm neonates that can be applied to transgenic mice.

Methods: The right common carotid artery of the neonatal mouse was ligated on postnatal day 3 (P3) C57BL/6 mice and followed by 80, 90, or 100 min of hypoxia using a mixture of 10%±0.2% oxygen-nitrogen. The most suitable model was chosen by characterizing the effects of this hypoxic-ischemic insult on development of myelin, glial cell conditions, and neurological outcomes by hematoxylin-eosin (HE) staining performed at postnatal day 17 (P17), western blot measuring myelin basic protein (MBP) at postnatal day 10 (P10) and P17, immunofluorescence staining of MBP-neurofilament protein heavy chain (NFH), oligodendrocyte transcription factor-2 (Olig2)-adenomatous polyposis coli clone (CC1), glial fibrillary acidic protein (GFAP) and ionic calcium linker protein (Iba-1) at P17, electron microscopy observing myelin microstructure at postnatal day 52 (P52) and behavioral testing at postnatal day 45–50 (P45–P50).

Results: The 90-min group showed neuroanatomical changes in the ipsilateral side of the brain, the 80-min group showed minor changes, and the 100-min group showed severe injury. Mice in the 90-min group subsequently showed marked activation of astrocytes, augmentation of microglia, a notable decrease in expression of MBP with a normal level of NFH, long-term cognitive dysfunction, and impairment of the myelin ultrastructure in adulthood.

Conclusions: In conclusion, a mouse model of preterm diffuse WMI rather than cystic periventricular leukomalacia was successfully achieved by ligating one of the common carotid arteries on P3 followed by 90 min of hypoxia in a mixture of 10%±0.2% oxygen-nitrogen. The attempt provides an adequate translational animal model for elucidating the underlying mechanism.

Keywords: White matter injury (WMI); hypoxia-ischemia (HI); preterm birth; myelin; mouse

Submitted Feb 19, 2022. Accepted for publication May 24, 2022.

doi: 10.21037/tp-22-58

View this article at: https://dx.doi.org/10.21037/tp-22-58

Introduction

Approximately 25–50% of survivors of premature birth show neurodevelopmental impairment in areas that include cognition, social behavior, attention, and learning disabilities as a result of brain injury (1,2). The spectrum of preterm brain injury has changed over time and diffuse white matter injury (WMI) is now the primary type of damage (3). Studies on postmortem brain tissue from preterm neonates indicated that myelination disorder occurring in WMI was associated with abnormal maturation of oligodendrocytes (4-6). In spite of proliferation of new oligodendrocyte precursor cells, subsequent glial scars formed by active astrocytes and microglia arrest the normal differentiation process toward maturation of these cells (7).

Several animal model mimicking WMI have been developed in an effort to determine the mechanisms of WMI. The time when humans are most susceptible to WMI is gestational age 23–32 weeks, which corresponds to postnatal day 1–3 (P1–P3) in rodents (8). However, most previous WMI models choose rodents at postnatal day 5–7 (P5–P7) (9-11). The WMI is classically related to two upstream mechanism that hypoxia-ischemia (HI) and inflammation/infection that sometimes coexist to produce injury (12). Although the mice model induced by interleukin-1 beta (IL-1β) from postnatal day 1 to postnatal day 4 (P1–P4) showed diffuse WMI (13). However, HI also plays an important role in the pathophysiology of preterm brain injury. The vulnerable white matter exposed to HI generates oxidative stress and excitotoxicity which then cause reactive gliosis and arrest the maturation of oligodendrocyte (14). Nowadays, transgenic mice can often provide rapid and cost-effective access to molecular and cellular mechanisms. Mice have shown great advantages on establishing disease model as it can be applied on the basis of genetically modified mice. Therefore, postnatal day 3 (P3) mouse pups were chosen for this investigation of whether or not a postnatal HI insult can induce preterm-like diffuse WMI resembling that seen clinically.

Our findings of loss of white matter, myelin deficiency, activation of glial cells, and long-term cognitive and learning disabilities in these mice reflect preterm-like diffuse WMI. We present the following article in accordance with the ARRIVE reporting checklist (available at https://tp.amegroups.com/article/view/10.21037/tp-22-58/rc).

Methods

Animals

Experiments were approved by the Animal Ethics Committee of Children's Hospital of Fudan University (No. 2020-239). Mice were treated in accordance with the National Institutes of Health (NIH) Guide for the Care and Use of Laboratory Animals. C57BL/6 mice at the reproductive stage were purchased from Shanghai Sippr-B&K Laboratory Animals Co. Ltd. (Shanghai, China). The newborn pups of these mice were used in the experiments performed in this study. The day of birth was defined as postnatal day 0 (P0). The mice were housed in the department of Laboratory Animal Science at Fudan University under specific pathogen-free conditions with a 12-h light/dark cycle and ad libitum access to food and autoclaved water. Pups remained with the dam until the day of HI injury.

HI protocol

On P3, C57BL/6 pups were randomly subjected to an HI insult or sham group. Pups were anesthetized with isoflurane and the right common carotid artery was double-ligated and severed (15). Total operating time was limited to 5 min. After a recovery period of 1 h, pups were placed in a container kept at 37 ℃ and exposed to hypoxia in humidified 10%±0.2% oxygen/nitrogen for 80, 90, or 100 min. Pups were then returned to their dams until they were euthanized. Sham mice's right common carotid artery were isolated, but not ligation, after anesthetized and stayed in incubator (normoxia) with relative time. Each mouse was observed twice a day to preserve them in health condition.

Histopathology

At 14 days after HI (postnatal day 17, P17), mice were deeply anesthetized and perfused with paraformaldehyde (PFA) before brain extraction. Serial coronal sections of 10-μm thickness were taken through corpus callosum and hippocampus using a rotary microtome and stained with hematoxylin-eosin (HE). To analyze brain volume, digitized images of coronal sections with millimetric ruler were obtained using Nikon Eclipse E100 and interfaced by a software Nikon DS-U3. A total of two sections per brain were used to evaluate the damage produced by the

HI insult using FIJI software. Volume assessment of cortex was produced from sections taken 0.2 and –2.4 mm from Bregma while hippocampal size was assessed from sections taken –2.4 mm from Bregma. Fifteen regions per section were randomly picked from corpus callosum to evaluate white matter thickness from sections taken 0.2 mm from Bregma. All sections were analyzed by an investigator who was blinded to the experimental groups.

Immunofluorescence

At 7 days after HI (postnatal day 10, P10) and P17, mice were deeply anesthetized with PFA before brain extraction. Then the brains were immersed in PFA for 24 h, and sequentially dehydrated with sucrose solution at 4 ℃. Coronal brain sections (30 μm) were cut using a cryostat (CM 1950; Leica, Nussloch, Germany). After washing in phosphate-buffered saline (PBS), free-floating tissue sections were saturated with blocking buffer for 1 h, and then incubated with the primary antibody, i.e., anti-myelin basic protein (MBP, 1:200, BioLegend, California, USA), anti-neurofilament protein heavy chain (NFH; 1:1,000, Abcam, Massachusetts, USA), anti-glial fibrillary acidic protein (GFAP, 1:200, Cell Signaling Technology, Boston, USA), anti-Iba1 (1:100, Abcam), anti-Olig2 (1:1,000, Novus Biologicals, Colorado, USA) and anti-CC1 (1:100, Merck, Darmstadt, Germany) overnight at 4 ℃. After rewarming for 30 min, the sections were rinsed and incubated for 1 h with the appropriate Alexa Fluor-conjugated secondary antibodies [anti-mouse IgG (H+L)-Cy2, anti-rabbit IgG (H+L)-Cy3, 1:500, Jackson ImmunoResearch, West Grove, USA] followed by 10 min DAPI counter staining. Sections were mounted using antifade mounting medium.

Defined non-overlapping regions of interest (ROI, each 348,100 μm^2) were visualized and photographed using a TCSSP8 fluorescence microscope. The fluorescent intensity of MBP, NFH and GFAP were calculated in a blinded manner using Image-Pro Plus 6.0 software (Media Cybernetics Inc., Rockville, MD, USA). Cell counting was performed manually using Fiji (https://imagej.net/Fiji) software. Criteria for cell inclusion were clear presence of a $DAPI^+$ nucleus, together with clear $Olig2^+$, $Olig2^+CC1^+$, Iba-1^+ staining. Two sections per brain were used to evaluate the fluorescent intensity in corpus callosum. To reduce the variability, sections were stained at the same time and photographed using the same exposure time setting, brightness and contrast for each fluorophore.

Western blotting

At P10 and P17, the HI injured brains were carefully removed as completed and rapidly as possible. The tissue was homogenized by a magnetic grinder in protein extract solution (T-PER Tissue Protein Extraction Reagent, Halt Protease Inhibitor Cocktail; Thermo Fisher Scientific, Waltham, MA, USA). The supernatants were reserved after centrifugation. Supernatant with 50 μg of total protein was then denatured at 95 ℃ for 5 min and separated using sodium dodecyl sulfate polyacrylamide gel electrophoresis (12%). Next, the protein was transferred to a nitrocellulose membrane and saturated for 2 h with blocking buffer (7% defatted milk) followed by the primary antibody (mouse anti-MBP, 1:1,000, BioLegend; mouse anti-actin, 1:1,000, Origene Technologies, Rockville, MD, USA) and incubation overnight at 4 ℃. After rewarming for 30 min, the membranes were incubated in the secondary antibody [goat anti-mouse IgG-horseradish peroxidase (HRP), 1:500; goat anti-rabbit IgG-HRP, 1:500, Absin, Shanghai, China] for 1 h. A ChemiDocXRS+ imaging system and ImageLab software (Bio-Rad, Hercules, CA, USA) were used for visualization and densitometric analysis after 5 min of immersion in enhanced chemiluminescence substrate (Thermo Fisher Scientific). The strips were analyzed using ImageLab version 5.0 (Bio-Rad).

Electron microscopy

On postnatal day 52 (P52), the corpus callosum was separated and post-fixed in a mixture of 4% PFA and 2.5% glutaraldehyde in 0.1 M phosphate buffer. Following dehydration with ethanol and embedding with epoxy resin, the samples were transferred to 0.1 M PBS and immersed in 1% OsO_4. Ultrathin (70-nm) sections were cut by ultramicrotome and placed onto copper grids. Finally, the sections were examined using a transmission electron microscope (JEM-1400, JEOL, Akishima-shi, Japan) after staining with uranyl acetate and lead citrate. The total numbers, the inner diameters (axon diameters) and outer diameters (fiber diameters) of myelinated axons in five non-overlapping random fields were measured manually using Fiji, and the g-ratio (inner diameter/outer diameter of each nerve fiber) was calculated (16).

Behavioral assessment

By comparing key developmental processes in brain across

humans and rodents, postnatal day 35–49 (P35–P49) mice are correspond to age 12–18 years of human (17). Behavioral test examined on postnatal day 45–50 (P45–P50) mice, reflected behaviors and brain functions of adolescent and adult mice. Open field test was performed at P45. The mice were acclimated in a quiet, darkened, and ventilated environment at a room temperature of 23–25 ℃ for 30 min without visualizing the device, which consisted of a transparent open box (dimensions 33×33×40 cm) in an airtight sound proofed test chamber covered with white paper. The mouse was placed gently in the middle of the box and a video recording (Shanghai JiLiang Software Technology Co. Ltd., Shanghai, China) was started. The behavior of the mouse, including total distance covered, time spent in the central area, and frequency of rearing, was recorded for 5 min.

Morris water maze, for learning and memory tests were performed on postnatal day 46–50 (P46–P50) mice. Pool provided by Shanghai Jiliang Software Technology Co. Ltd., was divided by marks into four quadrants. The environment was kept dimly lit and quiet at an air temperature at 23–25 ℃ and a water temperature controlled at 18–22 ℃. For the navigation test, the animals performed 4 trials daily for 4 consecutive days. During each trial, the mouse was allowed to swim for 60 s until it found the platform and remained there for 15 s. The movements within the maze were recorded. On day 5 (P50), the platform was removed and probe test was performed. The number of times the platform was crossed and the percentage of time spent in the target quadrant were analyzed.

Statistical analysis

The statistical analysis was performed using statistical package for Social Sciences version 20.0 and charted with GraphPad Prism version 7.0. Repeated measurements and the general linear model in the SPSS software were used to compare the sham and HI groups, except for analysis of the navigation test. The independent sample *t*-test was used, and in the event of unequal variance or a non-normal distribution, Welch's correction or the Mann-Whitney U test was applied. The data are presented as the mean with the standard deviation. A P value of <0.05 was considered statistically significant.

Results

Macrostructural and microstructural changes in brain white matter

The survival rate was 80% (16/20) in the group exposed to 80 min of hypoxia, 71.4% (15/21) in the group exposed to 90 min, and 45.8% (11/24) in the group exposed for 100 min. The ipsilateral brain volume was compared with that in the contralateral brain, and the degree of brain injury was classified as mild (barely any change in eye), moderate (volume loss less than one third), or severe (loss of more than one third or evidence of liquefactive necrosis). The brain injury was categorized as mild in 50% of cases and moderate in 43.8% in the 80-min group, as moderate in 53.3% and severe in 13.3% of cases in the 90-min group, and as moderate in 45.5% and severe in 27.3% of cases in the 100-min group (*Figure 1A*). MBP expression level corresponded with three degrees brain injury: compared to sham group, MBP expression in mild degree declined slightly and violently dropped in severe degree (*Figure 1A*). HE staining was performed for observing histological structure of the mouse brain (*Figure 1B*,*1C*). Cortical and hippocampal volume and thickness of corpus callosum were measured in ipsilateral hemisphere. Compared with the sham group, there was no significant change in the 80-min group (*Figure 1D*, P>0.05). In the 90-min group, the HI-insulted ipsilateral side showed slight atrophy in gross with ventricular enlargement, but no significant changes in cortical volume (P>0.05, *Figure 1A*,*1C*,*1D*). Thickness of corpus callosum decreased significantly with disorganized structure and visible karyopyknosis (P<0.01). The hippocampal volume varied among samples, swelling or shrinking, without a statistically significant difference compared with the sham group (P>0.05). Volume reduction and disorganization of hippocampus pyramidal cell layer were observed under high magnification. The most severe injury was evident in the 100-min group, including excessive ventricular enlargement, remarkable decrease in cortical volume (P<0.01) and reduced thickness of corpus callosum (P<0.001). Since 1/2 samples in the 100-min group lost the entire hippocampus, hippocampal volume in this group was not statistically analyzed and displayed in *Figure 1A-1C*.

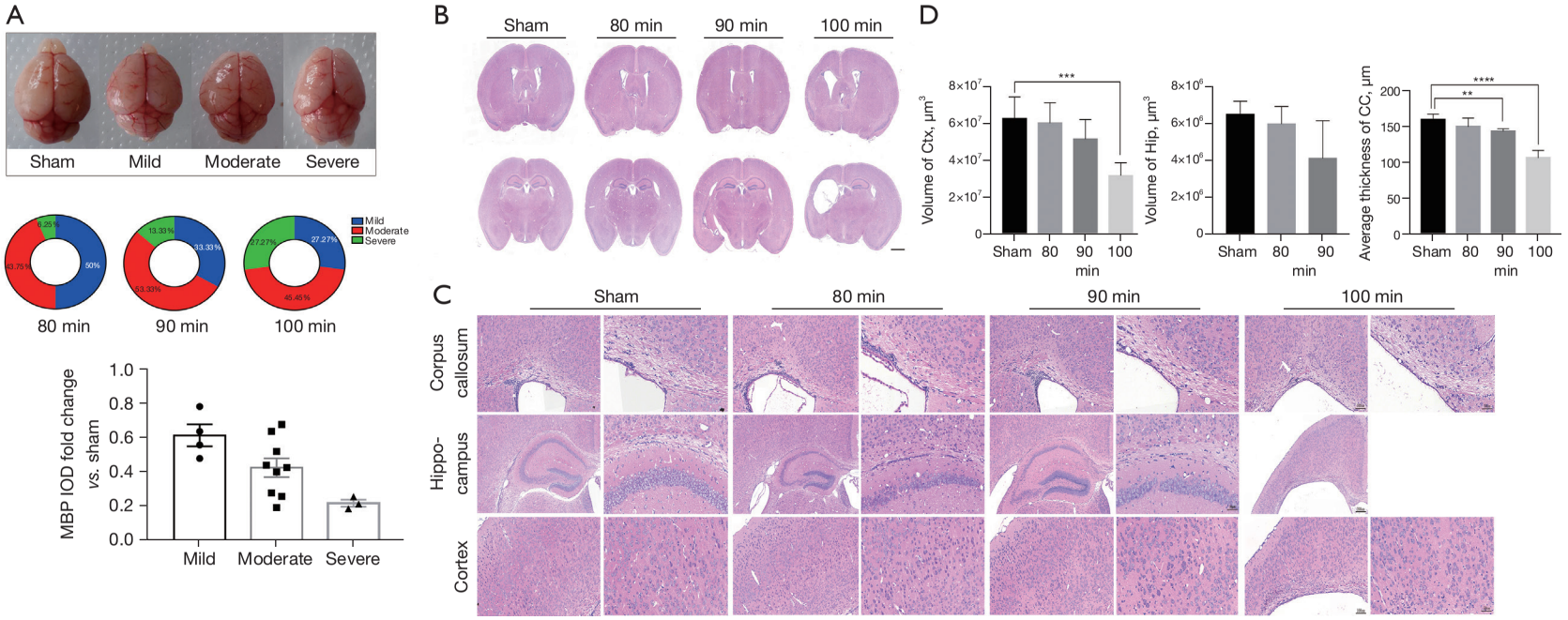

Figure 1 Macrostructural and microstructural changes in the mouse brain after HI injury at P17. (A) Representative photographs of different degrees of brain injury (upper panel), a stacked percentage column showing three injury degrees promotion in three groups (middle panel) and a scatter diagram showing tendency of MBP expression level among different brain injury degrees (lower panel). (B) Representative photographs of coronal brain sections with HE staining in the sham-operated, 80-, 90-, and 100-min groups. Scale bar: 1 mm. (C) Representative photographs of the HE-stained brain sections of the cortex, CC and hippocampus. Scale bar: cortex and CC, left: 100 μm, right: 50 μm; hippocampus, left: 200 μm; right: 50 μm. (D) Statistical analysis in cortex volume, thickness of CC and hippocampus volume. n=6 mice/group. sham: without HI; 80 min: HI with hypoxia for 80 min group; 90 min: HI with hypoxia for 90 min group; 100 min: HI with hypoxia for 100 min group. **, P<0.01; ***, P<0.001; ****, P<0.0001. MBP, myelin basic protein; IOD, integrated optical density; HI, hypoxia-ischemia; CC, corpus callosum; P17, postnatal day 17; HE, hematoxylin-eosin.

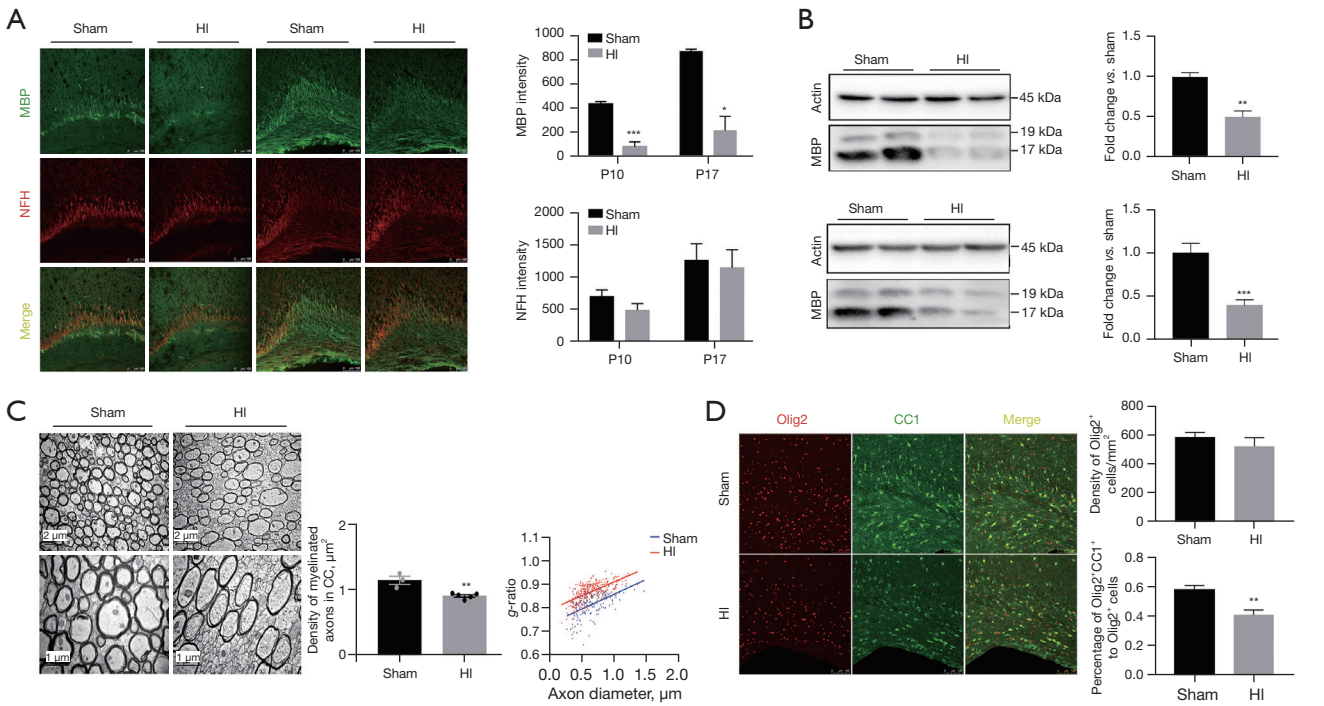

Figure 2 Impaired myelination with arrested oligodendrocyte maturation in the 90-min group. (A) Representative photographs of (green) MBP-NFH (red) co-staining at P10 (left) and P17 (right). Scale bar: 100 μm. (B) Western blot images and quantification of MBP at P10 (upper panel) and P17 (lower panel). (C) Representative electron microscopy photographs at P52. Histograms for the densities of myelinated axons and the g-ratio plotted versus axon diameters of the CC. Scale bar: 2 μm (upper panel), 1 μm (lower panel). (D) External capsule of sham *vs.* HI mice stained for Olig2 (red) CC1 (green). Olig2$^+$ represents oligodendrocyte lineage cells and Olig2$^+$CC1$^+$ indicate mature oligodendrocytes. Scale bar: 100 μm. n=5–6 mice/group. sham: without HI. *, P<0.05; **, P<0.01; ***, P<0.001. MBP, myelin basic protein; NFH, neurofilament protein heavy chain; HI, hypoxia-ischemia; P10, postnatal day 10; P17, postnatal day 17; CC, corpus callosum; P52, postnatal day 52.

Myelination disorder with impaired maturation of oligodendrocytes

MBP is an essential structural protein for myelination and NFH is a marker of maturation of neuronal axons (15). At P10 and P17, MBP protein expression was detected by western blot and immunofluorescence staining. NFH was used as a co-stain to observe the development of nerve axons. Compared with the sham group, there was no significant difference in MBP expression in the 80-min group (data not shown); however, there was a significant reduction in MBP expression in the 90-min group (*Figure 2A*,*2B*, P<0.05). The western blot and staining results showed a marked decrease in the MBP protein level in the ipsilateral hemisphere, with no signs indicating a change in NFH expression (*Figure 2A*,*2B*).

Then we analyzed the structure and density of myelin in the corpus callosum in the 90-min group at postnatal day 52 (P52) by electron microscopy to further assess the effects of HI injury on long-term myelination in the mice. Electron microscopy revealed that the numbers of myelinated axons in the HI group were markedly decreased relative to the sham group (P<0.05, *Figure 2C*, top panel). Meanwhile, the myelinated axons in the HI group appeared to be loosely wrapped and the myelin g-ratio was significantly higher than the shams (P<0.01, *Figure 2C*, bottom panel) indicating that the thicknesses of myelin sheaths also reduced.

Co-staining for CC1 (a marker of mature oligodendrocytes) and Olig2 (a nuclear oligodendrocyte marker) was performed at P17 to investigate maturation of oligodendrocyte lineage cells (*Figure 2D*). Compared with the sham group, there was no difference in the density of Olig2$^+$ cells in corpus callosum in the HI group (P>0.05); however, there was an obvious decrease in the proportion of mature oligodendrocytes (ratio of Olig2$^+$CC1$^+$cells to Olig2$^+$cells, P<0.01).

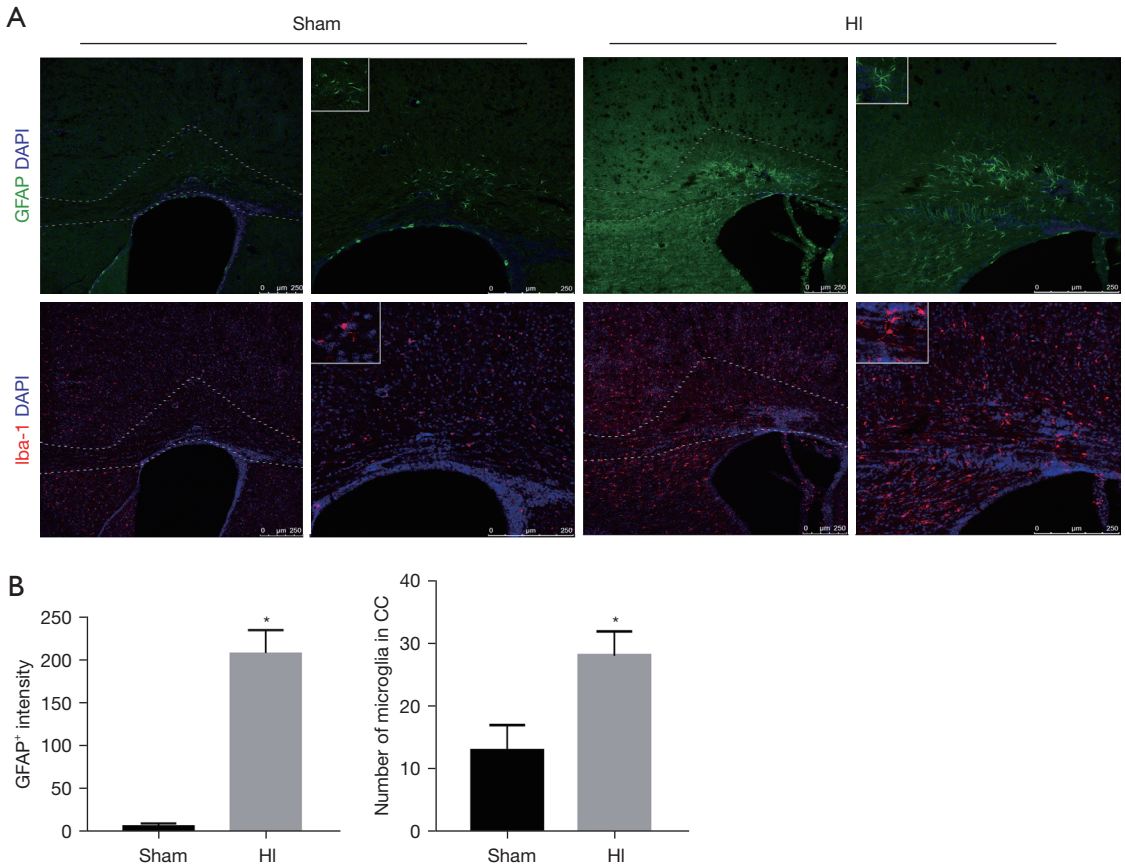

Figure 3 Activation of astrocytes and microglia after hypoxic-ischemic insult in mice. (A) Representative images of brain sections staining for the astrocyte marker GFAP (green), the microglia marker Iba-1 (red), and the nuclear marker DAPI (blue). The right side of each panel show higher magnification of the left side. The area outlined on the left side is the CC. The boxed area on the right side shows magnified morphology of astrocytes and microglia. Scale bar: 250 μm. (B) Quantification of GFAP$^+$ intensity (left). The number of microglia increased in CC area (right panel). n=5–8 mice/group. sham: without HI. *, P<0.05. HI, hypoxia-ischemia; GFAP, glial fibrillary acidic protein; CC, corpus callosum.

Activation of astrocytes and microglia after HI insult in mice

To investigate whether or not glia cells are activated in immature mice after the HI insult, brain sections taken at P17 in the 90-min group were stained for GFAP, an astrocyte marker, and Iba1, a microglia marker (*Figure 3A*). Compared with the sham group, there was a significant increase influorescence intensity of GFAP (P<0.05, *Figure 3B*, upper panel). Astrocytes, which were characterized by hypertrophy and hyperplasia, were obviously reactive in the corpus callosum and cingulate area. Furthermore, Iba1-positive microglia were distributed widely in the corpus callosum, cortical area, and a granular insular cortex. However, compared with the sham group, the only area difference in the number of microglia was in the ipsilateral corpus callosum (P<0.05, *Figure 3B*, lower panel). Besides, a more amoeboid morphology of microglia was observed with increasing cell circularity, more than three hypertrophied protuberances.

Animal behavior tests for evaluating brain function

At P45, mice were subjected to the open field test (data for the 90-min group are shown in *Figure 4A*). The results indicated that the HI group spent a longer time in the central area than did the sham group; however, the difference was not statistically significant (P>0.05). HI mice were still considered having a larger tendency to anxiety

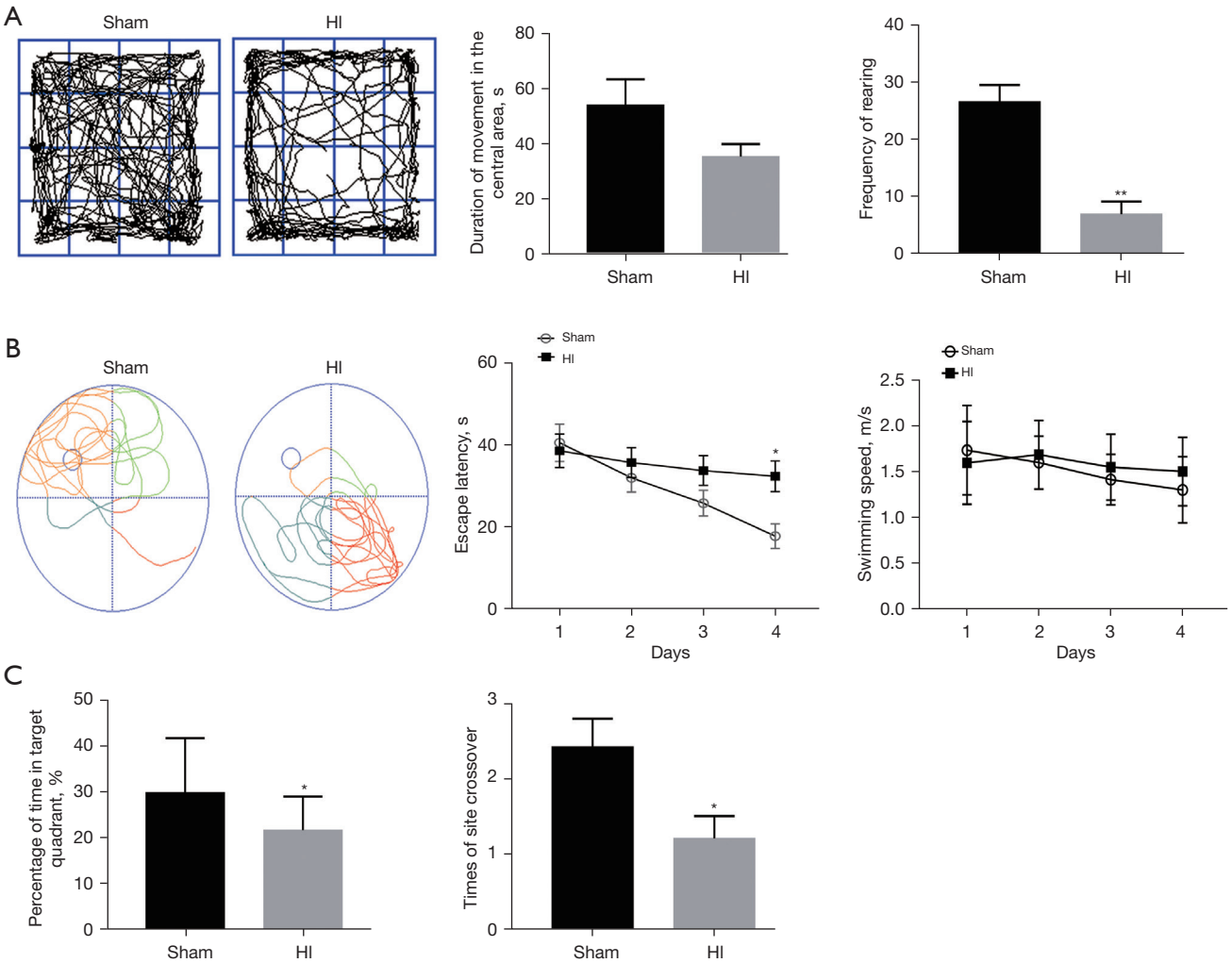

Figure 4 Animal behavior tests for evaluating functional consequences of an HI insult in mice. (A) Representative total tracks in the open field test and quantification of duration of movement in the central area representing anxiety as well as frequency of rearing representing exploration tendency. There were no significant changes in the former but there was a decrease in the latter. (B) Swim path traces from the probe test of the Morris maze. A learning ability deficit in the HI group is shown by prolonged escape latency on day 4. No difference in swimming speed indicates general normal motor function. (C) In the probe trial, reduction in space memory ability was shown in a lower percentage of time spent in the target quadrant and fewer platform crossovers. n=8–17 mice/group. sham: without HI. *, P<0.05; **, P<0.01. HI, hypoxia-ischemia.

and the no difference in data may owe to the assessment of anxiety level of mice were still easily disturbed, although they were familiar to the researchers and were acclimated to the environment. However, the frequency of rearing (both front paws off the ground, with front paws against a wall or standing) was markedly lower in the HI group than in the sham group (P<0.01).

Escape latency in the Morris water maze (*Figure 4B,4C*) decreased in both groups from day 1 to day 4 in the navigation test (postnatal day 46–49, P46–P49), suggesting that these mice possessed some degree of learning ability. The escape latency of mice in the HI group was longer than that in the sham group; the difference was statistically significant on day 4 (P<0.05). However, there was no difference in swimming speed (P>0.05).

In the water maze probe trials performed on the second

day after the navigation test (P50), the HI mice spent less time in the target quadrant and crossed the platform significantly more times than did the mice in the sham group ($P<0.05$).

Discussion

Diffuse WMI is the predominant pattern of brain injury observed in contemporary cohorts of preterm infant (18). A volume reduction and abnormal microstructural in white matter, ventriculomegaly, hippocampus volume changes and impaired gyral development can be seen through magnetic resonance imaging or cranial ultrasound (18-20).

Macrostructural observations outlined the injury degrees situations among different hypoxic-time groups, helping to select appropriate HI scheme. Combining the results of ipsilateral brain volume loss and HE staining of brain sections, the 90-min group showed moderate neuroanatomic changes, including a thinner corpus callosum and disorganized hippocampus structure, without significant volume changes in cortex and hippocampus, whereas no significant changes were noted in the 80-min group and major damage was observed in the 100-min group. Given that non-necrotic diffuse WMI is the predominant form of preterm WMI, unilateral carotid artery ligation followed by 90 min of hypoxia in 10%±0.2% oxygen/nitrogen was considered adequate for inducing mainly WMI with mild grey matter injury.

MBP is the most important constitutive protein of myelin, which reflect the formation of myelin sheaths on the protein level (21). NFH is the main skeleton protein of neuron axons, which is usually used to identify axons (21). The normal expression level of MBP detected through western blot in the 80-min group mice indicated again that this scheme was not sufficient to cause significant injury to the myelin structure. The decreased expression levels of MBP in the 90-min group at P10 and P17 reflected the lack of constitutive protein of myelin, indicating that myelination at this time was disrupted or delayed. Furthermore, decrease of myelinated axons number and reduction of myelin sheath thickness observed through electron microscopy at P52, indicated that myelination disorder was still exist in adulthood of mice. However, normal NFH expressions at P10 and P17 indicate that the axons developed as normal at this time.

Analysis based on autopsy series data indicated that oligodendrocyte progenitors (pre-OLs) regenerate but survive in a state of arrested maturation that reduces the pool of oligodendrocytes available for myelination after selective degenerate in acute stage of injury (4). In addition, diffuse astrogliosis and microglial activation are the major pathological feature of WMI and were demonstrated to be involved in the mechanism of the pre-OLs injury (22). Olig2, a key fate-determining transcription factor of the oligodendrocyte lineage, is expressed by all oligodendrocytes and $CC1^+Olig2^+$ cells indicate mature oligodendrocytes (23,24). In this mouse model, when compared with the sham group, the oligodendrocyte lineage cell ($Olig2^+$ cell) density showed no significant change in the HI group but the proportion of mature oligodendrocytes ($Olig2^+CC1^+$cells) was obviously lower, indicating oligodendrocyte maturation was impaired. Meanwhile, activation of astrocytes and microglia in the white matter were also observed.

Several previous studies have revealed that diffuse WMI is often associated with neurologic impairment, such as cognitive function and an increased risk of psychological disorders (25,26). In this study, we investigated brain function in this mouse model using animal behavior tests. The open field test indicated a decrease in exploratory behavior and long-term cognitive dysfunction, including learning and memory abilities impairment, were detected in the Morris water maze test.

Therefore, our results suggest that unilateral ligation of the common carotid artery followed by 90 min of hypoxia in a 10% nitrogen-oxygen mixture can induce diffuse WMI in P3 C57BL/6 mice, which more comparable to the WMI infants seen in clinical practice: hypomyelination, oligodendrocytes maturation arrest, activation of astrocytes and microglia and long-term cognitive and psychological disorder (4,19,26). HI, inflammation or incorporation of the two were mostly used to induce diffuse WMI (13,27). The utility of mice pups with lipopolysaccharide (LPS) or IL-1β-induced inflammation were to mimic inflammation induced diffuse WMI which failed to assess long term psychological and cognitive function (13,28). We also find variability between diffuse WMI mice model induced by HI in different parameters, such as postnatal day of the mice, the percentage of oxygen, the time exposure to hypoxia, and the of ligation unilateral common carotid artery (27). Our finding is different from that in previous HI models of immature mouse, which mostly chose postnatal 5 as the target point for hypoxia and resulted in a mass of gray matter necrosis or axonal degeneration, which is not commonly associated with preterm WMI unless white matter involves severe necrosis (8). By comparing the fundamental brain development processes that occur in both

rodents and humans, brain development stage of P1–P3 mice is corresponds to human gestational age 23–32 weeks, a stage when HI-sensitive pre-OLs are the predominant cells in white matter. As described before, the aim of this paper is to establish a more clinically relevant and robust model of preterm brain injury in mice, as transgenic mice can often provide rapid and cost-effective access to molecular and cellular mechanisms.

Conclusions

In summary, a comprehensive verification procedure was performed to confirm that our mouse model is consistent with the clinical characteristics of diffuse WMI in preterm neonates. This translational animal model is suitable for use by researchers investigating the mechanism underlying diffuse WMI.

Acknowledgments

Funding: This work was supported by the National Key R&D Program of China (grant numbers 2017YFA0104200) and National Natural Science Foundation of China (grant number 82001596).

Footnote

Reporting Checklist: The authors have completed the ARRIVE reporting checklist. Available at https://tp.amegroups.com/article/view/10.21037/tp-22-58/rc

Data Sharing Statement: Available at https://tp.amegroups.com/article/view/10.21037/tp-22-58/dss

Conflicts of Interest: All authors have completed the ICMJE uniform disclosure form (available at https://tp.amegroups.com/article/view/10.21037/tp-22-58/coif). The authors have no conflicts of interest to declare.

Ethical Statement: The authors are accountable for all aspects of the work in ensuring that questions related to the accuracy or integrity of any part of the work are appropriately investigated and resolved. Experiments were approved by the Research Ethics Board of the Children's Hospital of Fudan University (No. 2020-239), and mice were treated in accordance with the National Institutes of Health Guide for the Care and Use of Laboratory Animals.

References

1. Vanes LD, Murray RM, Nosarti C. Adult outcome of preterm birth: Implications for neurodevelopmental theories of psychosis. Schizophr Res 2021. [Epub ahead of print]. doi: 10.1016/j.schres.2021.04.007.
2. Cayam-Rand D, Guo T, Synnes A, et al. Interaction between Preterm White Matter Injury and Childhood Thalamic Growth. Ann Neurol 2021;90:584-94.
3. Murray AL, Thompson DK, Pascoe L, et al. White matter abnormalities and impaired attention abilities in children born very preterm. Neuroimage 2016;124:75-84.
4. Buser JR, Maire J, Riddle A, et al. Arrested preoligodendrocyte maturation contributes to myelination failure in premature infants. Ann Neurol 2012;71:93-109.
5. Volpe JJ, Kinney HC, Jensen FE, et al. The developing oligodendrocyte: key cellular target in brain injury in the premature infant. Int J Dev Neurosci 2011;29:423-40.
6. Back SA. Perinatal white matter injury: the changing spectrum of pathology and emerging insights into pathogenetic mechanisms. Ment Retard Dev Disabil Res Rev 2006;12:129-40.
7. van Tilborg E, de Theije CGM, van Hal M, et al. Origin and dynamics of oligodendrocytes in the developing brain: Implications for perinatal white matter injury. Glia 2018;66:221-38.
8. Vaes JEG, Vink MA, de Theije CGM, et al. The Potential of Stem Cell Therapy to Repair White Matter Injury in Preterm Infants: Lessons Learned From Experimental Models. Front Physiol 2019;10:540.
9. van Tilborg E, Heijnen CJ, Benders MJ, et al. Impaired oligodendrocyte maturation in preterm infants: Potential therapeutic targets. Prog Neurobiol 2016;136:28-49.
10. Zaghloul N, Kurepa D, Bader MY, et al. Prophylactic inhibition of NF-κB expression in microglia leads to attenuation of hypoxic ischemic injury of the immature brain. J Neuroinflammation 2020;17:365.
11. Zeng Y, Wang H, Zhang L, et al. The optimal choices

of animal models of white matter injury. Rev Neurosci 2019;30:245-59.
12. Ophelders DRMG, Gussenhoven R, Klein L, et al. Preterm Brain Injury, Antenatal Triggers, and Therapeutics: Timing Is Key. Cells 2020;9:1871.
13. Stolp HB, Fleiss B, Arai Y, et al. Interneuron Development Is Disrupted in Preterm Brains With Diffuse White Matter Injury: Observations in Mouse and Human. Front Physiol 2019;10:955.
14. Schneider J, Miller SP. Preterm brain Injury: White matter injury. Handb Clin Neurol 2019;162:155-72.
15. Wang MJ, Li ZH, Gao RW, et al. Effects of delayed HIF-1α expression in astrocytes on myelination following hypoxia-ischaemia white matter injury in immature rats. Transl Pediatr 2022;11:20-32.
16. RUSHTON WA. A theory of the effects of fibre size in medullated nerve. J Physiol 1951;115:101-22.
17. Semple BD, Blomgren K, Gimlin K, et al. Brain development in rodents and humans: Identifying benchmarks of maturation and vulnerability to injury across species. Prog Neurobiol 2013;106-107:1-16.
18. Agut T, Alarcon A, Cabañas F, et al. Preterm white matter injury: ultrasound diagnosis and classification. Pediatr Res 2020;87:37-49.
19. Malavolti AM, Chau V, Brown-Lum M, et al. Association between corpus callosum development on magnetic resonance imaging and diffusion tensor imaging, and neurodevelopmental outcome in neonates born very preterm. Dev Med Child Neurol 2017;59:433-40.
20. Strahle JM, Triplett RL, Alexopoulos D, et al. Impaired hippocampal development and outcomes in very preterm infants with perinatal brain injury. Neuroimage Clin 2019;22:101787.
21. Yu X, Wu H, Zhao Y, et al. Bone marrow mesenchymal stromal cells alleviate brain white matter injury via the enhanced proliferation of oligodendrocyte progenitor cells in focal cerebral ischemic rats. Brain Res 2018;1680:127-36.
22. Back SA. White matter injury in the preterm infant: pathology and mechanisms. Acta Neuropathol 2017;134:331-49.
23. Tang J, Liang X, Dou X, et al. Exercise rather than fluoxetine promotes oligodendrocyte differentiation and myelination in the hippocampus in a male mouse model of depression. Transl Psychiatry 2021;11:622.
24. Ma R, Chu Y, Dou M, et al. Matrine inhibits the Wnt3a/β-catenin/TCF7L2 signaling pathway in experimental autoimmune encephalomyelitis. J Neuroimmunol 2022;367:577876.
25. You J, Yang HJ, Hao MC, et al. Late Preterm Infants' Social Competence, Motor Development, and Cognition. Front Psychiatry 2019;10:69.
26. Jansen L, van Steenis A, van den Berg-Huysmans AA, et al. Associations between Neonatal Magnetic Resonance Imaging and Short- and Long-Term Neurodevelopmental Outcomes in a Longitudinal Cohort of Very Preterm Children. J Pediatr 2021;234:46-53.e2.
27. Torres-Cuevas I, Corral-Debrinski M, Gressens P. Brain oxidative damage in murine models of neonatal hypoxia/ischemia and reoxygenation. Free Radic Biol Med 2019;142:3-15.
28. Vaes JEG, van Kammen CM, Trayford C, et al. Intranasal mesenchymal stem cell therapy to boost myelination after encephalopathy of prematurity. Glia 2021;69:655-80.

Cite this article as: Chen Q, Zhang K, Wang M, Gao R, Wang Q, Xiao M, Chen C. A translational mouse model for investigation of the mechanism of preterm diffuse white matter injury. Transl Pediatr 2022;11(7):1074-1084. doi: 10.21037/tp-22-58